Available online at www.sciencedirect.com
ScienceDirect
Journal of Sound and Vibration 305 (2007) 891–903
JOURNAL OF SOUND AND VIBRATION
www.elsevier.com/locate/jsvi

Short Communication

Adaptive vibration control using a virtual-vibration-absorber controller

Shang-Teh Wu*, Ying-Jhe Shao

Department of Mechanical Engineering, National Yunlin University of Science & Technology, Touliu, Yunlin 640, Taiwan

Received 23 September 2006; received in revised form 10 April 2007; accepted 21 April 2007
Available online 12 June 2007

Abstract

A control algorithm emulating a dynamic vibration absorber (DVA) is developed for a flexible structure subject to harmonic disturbances of uncertain frequency. The virtual vibration absorber is mathematically equivalent to a passive DVA, but its stiffness, inertia and damping coefficient are adjustable by software. Stiffness of the virtual spring is tuned according to the phase difference between the acceleration of the primary body and the displacement of the virtual mass. The adaptation algorithm consists of a phase detector with a low-pass filter, similar to that found in a phase-locked loop. Both undamped and damped vibration absorbers are developed; the former has the advantage of cleaner vibration neutralization while the latter has a smoother stiffness adaptation. Adaptation rate of the virtual stiffness is analyzed in detail. The effectiveness of the proposed method is confirmed by simulations and real-time experiments.

1. Introduction

Dynamic vibration absorbers (DVA) are a classic scheme for neutralizing harmonic excitations of a specified frequency. Properly tuned, an undamped DVA can ideally nullify the effect of external disturbances. To broaden the scope of applications various designs have been developed to make the DVA's characteristics tunable on-line. Many such schemes can be categorized as *adaptive passive* methods, in which the stiffness of a passive vibration absorber is adjusted automatically. The methods include adjustment of various flexible elements: the effective coil numbers of a mechanical spring [1], the length of threaded flexible rods by stepping motors [2], the shape of a flexible beam [3], the curvature of two parallel beams [4], and the effective length of a flexible beam by a moving support [5]. A non-contact scheme for changing stiffness instantly was presented in Ref. [6] by varying the strength of electromagnetic force. Recently "smart materials" such as shape memory alloy (SMA) [7,8] and magnetorheological (MR) elastomers (the structural solid analogue of MR fluids) [9] were also employed to serve as variable stiffness elements. Various control methods can be used for stiffness tuning in an adaptive passive vibration absorber, such as PD control, fuzzy

*Corresponding author. Tel.: +886 5 5342601 4111; fax: +886 5 5312062.
E-mail address: wust@yuntech.edu.tw (S.-T. Wu).

0022-460X/$ - see front matter © 2007 Elsevier Ltd. All rights reserved.
doi:10.1016/j.jsv.2007.04.046

logic [3,8,10], and PI control with integrator anti-windup [7]. In Ref. [7] an explicit stability analysis was presented for the adaptive algorithm.

Active vibration absorbers are mostly *hybrid* in the sense that passive flexible elements work alongside the active components to share the counter-disturbance efforts. Unlike adaptive passive systems, the actuators in active vibration control directly counterbalance at least part of the external force. These actuators include linear motors with air springs [11], electromagnetic actuators [12], piezoceramic inertial actuators [13], electrohydraulic actuators [14] and linear voice-coil motors [15]. The control methods include classical full-state feedback controls [16], state feedback with frequency-shaped functional [11], neural networks [17], and a delayed resonator using a time-delayed position feedback [12].

In this paper, a virtual passive approach is adopted in the design of an adaptive vibration absorber. A virtual DVA can be emulated by a servomotor [18,19] or a linear actuator [20]. It is mathematically equivalent to a damped or undamped DVA, but the stiffness, inertia and damping coefficient can be readily adjusted by varying the parameters associated with the virtual elements. This approach is featured by simple control algorithms and is capable of realizing hard-to-implement mechanical designs, such as a symmetric pair of vibration absorbers with a sky-hooked spring [18], a multimode DVA for multi-frequency disturbances [19], and a sky-hooked damper as shown in this paper. The proposed method is an adaptive version of the scheme presented in Ref. [20], in which a fixed-gain, hybrid vibration absorber was explored. The virtual spring will be tuned according to the phase difference between the acceleration of the primary body and the displacement of the virtual mass; the latter is generated and updated in the computer while the former is measured by an accelerometer. The adaptation algorithm consists of a phase detector with a low-pass filter, similar to that found in a phase-locked loop (PLL). Dynamics of the virtual stiffness under the adaptation algorithm will be analyzed in detail based on a quasi-static assumption. That is, the adaptation rate is assumed to be much slower than the system's bandwidth. Simulations and experimental results are presented to demonstrate the performance of the proposed method.

2. Adaptive undamped vibration absorber

2.1. Virtual-passive vibration absorber

Fig. 1a shows an actively controlled mass–spring structure subject to a harmonic disturbance. The governing equation is as follows:

$$m\ddot{y} + ky = u + d, \tag{1}$$

where y is the displacement of the primary body, m is the inertia, k is the stiffness, u is the control input, and d is a harmonic disturbance of radian frequency ω_0. The linear actuator can be programmed to emulate a DVA by the following feedback algorithm:

$$u = k_a(z - y) - b\dot{y}, \tag{2}$$

$$\ddot{z} = \frac{k_a}{m_a}(y - z), \tag{3}$$

where z is the displacement of the virtual mass of inertia m_a, and k_a is the stiffness of the virtual spring. The derivative term $b\dot{y}$ is included to emulate a damper that is required to stabilize the system, since damping of the original structure is assumed to be negligible. Fig. 1b shows the equivalent mechanical structure for the closed-loop system of Eqs. (1)–(3). When the characteristic frequency of the virtual DVA is tuned to be $\sqrt{k_a/m_a} = \omega_0$, the harmonic disturbance will be completely neutralized.

2.2. Adaptive virtual vibration absorber

The fixed-gain virtual-vibration-absorber algorithm of Eqs. (2)–(3) is inadequate if the disturbance frequency is uncertain or is drifting over time. An adaptive scheme based on the phase difference between the accelerations of the primary body and the displacement of the virtual mass is developed below. It is noted that the disturbance frequency can also be accurately determined by a fast Fourier transform (FFT) spectrum

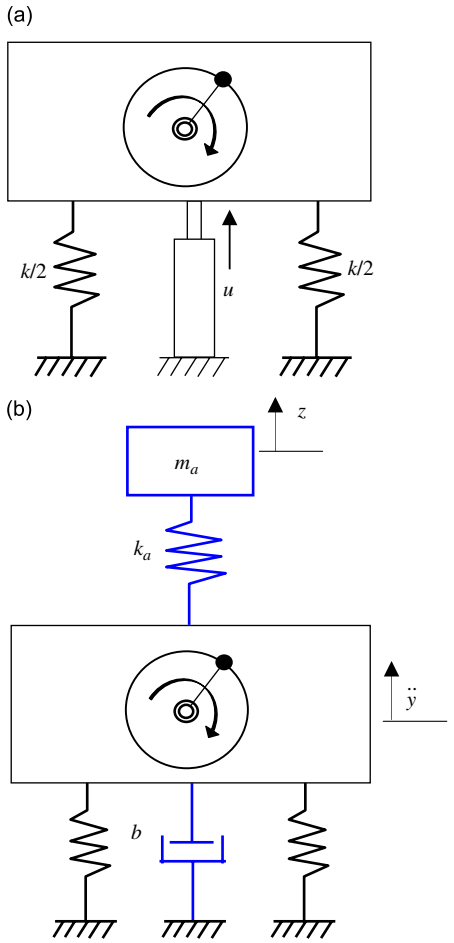

Fig. 1. (a) An actively controlled mechanical structure subject to harmonic disturbances; (b) a virtual dynamic vibration absorber emulated by the linear actuator.

analysis. However, it requires gathering of a block of data before the transform is conducted. Intensive computation is needed at periodic instants of time when, say, 1024 sampling data are accumulated. In contrast the proposed method updates the stiffness of the absorber progressively, sample by sample. The adaptation effort is thus distributed evenly over time, making it possible to simultaneously calculate the control input and adapt the characteristic frequency of the vibration absorber. As the stiffness is being adjusted, the oscillations are also gradually reduced.

Fig. 2 depicts the vibration control system where the stiffness of the virtual spring, k_a, is adjusted by a phase detector and a low-pass filter. The tuning rule is as follows:

$$\dot{k}_a = \gamma\psi, \tag{4}$$

$$\dot{\psi} = -\alpha\psi + \alpha\phi_d, \tag{5}$$

$$\phi_d = \frac{\ddot{y}}{\ddot{y}_{\text{rms}}}\frac{z}{z_{\text{rms}}}, \tag{6}$$

where ϕ_d is the phase detector for the displacement of the virtual mass and the acceleration of the primary body, ψ is the filtered value of ϕ_d, and γ is a positive constant that determines the updating rate. The subscript "rms" denotes the root mean square value of the signals: $\ddot{y}_{\text{rms}}$ (or z_{rms}) equals $\frac{1}{\sqrt{2}}$ the amplitude of $\ddot{y}$ (or z). As will be explained later, the adaptation rate can be set independently of the magnitude of the disturbance by

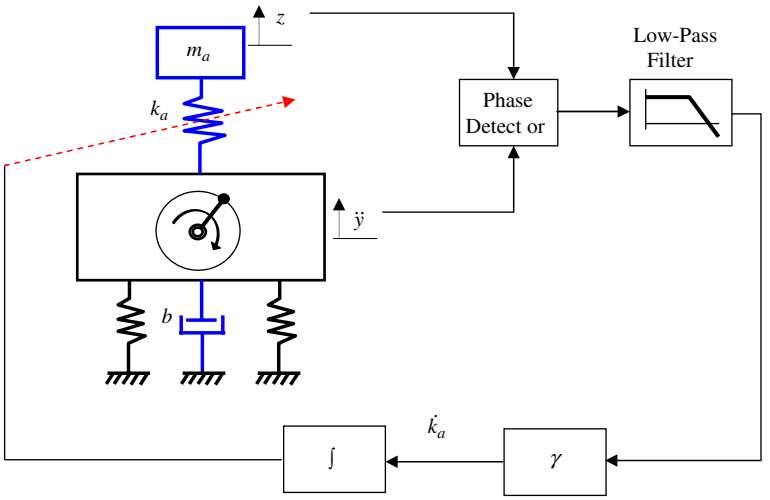

Fig. 2. Adaptive virtual vibration absorber with a phase detector.

normalizing the signals against their RMS values. In implementation the RMS value is estimated via a low-pass filter:

$$v_{\text{rms}} = \sqrt{w}, \tag{7}$$

$$\frac{\mathrm{d}w}{\mathrm{d}t} = -\alpha_1 w + \alpha_1 v^2, \tag{8}$$

where v stands for z or $\ddot{y}$, and α_1 is a positive value smaller (5–10 times smaller) than the nominal frequency of the disturbance. The adaptation rate of k_a from Eqs. (4)–(6) is analyzed below.

From Eq. (3) the transfer function from $\ddot{y}$ to z is obtained to be

$$\frac{z}{\ddot{y}} = \frac{k_a}{s^2(m_a s^2 + k_a)}. \tag{9}$$

At the frequency ω_0,

$$z = \frac{-k_a}{\omega_0^2(k_a - m_a\omega_0^2)}\ddot{y}. \tag{10}$$

Let

$$\ddot{y} = a_y \sin\omega_0 t,$$

where a_y denotes the amplitude; then from Eq. (10),

$$z = -a_z \sin(\omega_0 t - \theta),$$

where

$$a_z = \frac{k_a}{\omega_0^2|k_a - m_a\omega_0^2|}a_y$$

and

$$\theta = \begin{cases} 0 & \text{if } k_a/m_a > \omega_0^2, \\ \pi & \text{if } k_a/m_a < \omega_0^2, \\ \frac{1}{2}\pi & \text{if } k_a/m_a = \omega_0^2. \end{cases} \tag{11}$$

Since the RMS value equals $\frac{1}{\sqrt{2}}$ the amplitude, the product of normalized z and normalized $\ddot{y}$ can be arranged to be

$$\frac{z}{z_{\text{rms}}}\frac{\ddot{y}}{\ddot{y}_{\text{rms}}} = -\sqrt{2}\sin(\omega_0 t)(\sqrt{2})\sin(\omega_0 t-\theta)$$
$$= 2\sin(\omega_0 t)\cos(\omega_0 t-\phi), \tag{12}$$

where

$$\phi = \theta - \frac{\pi}{2}, \tag{13}$$

such that (from Eq. (11))

$$\phi = \begin{cases} -\pi/2 & \text{if } k_a/m_a > \omega_0^2, \\ +\pi/2 & \text{if } k_a/m_a < \omega_0^2, \\ 0 & \text{if } k_a/m_a = \omega_0^2. \end{cases} \tag{14}$$

By using the trigonometric identity,

$$\cos(\omega_0 t-\phi) = \cos(\omega_0 t)\cos\phi + \sin(\omega_0 t)\sin\phi.$$

Eq. (12) can be arranged to be

$$2\sin(\omega_0 t)\cos(\omega_0 t-\phi) = 2\sin(\omega_0 t)\cos(\omega_0 t)\cos\phi + 2\sin^2(\omega_0 t)\sin\phi$$
$$= \sin(2\omega_0 t)\cos\phi - \cos(2\omega_0 t)\sin\phi + \sin\phi. \tag{15}$$

From Eq. (15), $\sin\phi$ can be obtained by filtering out the high-frequency components of the normalized product of z and $\ddot{y}$. That is, if α is chosen to be much smaller than the frequency of the disturbance (α being 5–10 times smaller than ω_0), Eqs. (5)–(6) can be approximated by

$$\dot{\psi} = -\alpha\psi + \alpha\sin\phi. \tag{16}$$

Define

$$\delta k_a = k_a - k_a^*, \tag{17}$$

where k_a^* is the target value for k_a, i.e., $k_a^*/m_a = \omega_0^2$. From Eq. (4), it follows that

$$\frac{\mathrm{d}}{\mathrm{d}t}\delta k_a = \gamma\psi. \tag{18}$$

Differentiating Eq. (18) one more time and using Eq. (16), we have

$$\frac{\mathrm{d}^2}{\mathrm{d}t^2}\delta k_a = -\gamma\alpha\psi + \gamma\alpha\sin\phi. \tag{19}$$

From Eq. (14) and using Eq. (18) again, Eq. (19) can be written to be

$$\frac{\mathrm{d}^2}{\mathrm{d}t^2}\delta k_a + \alpha\frac{\mathrm{d}}{\mathrm{d}t}\delta k_a + \gamma\alpha\,\mathrm{sgn}(\delta k_a) = 0, \tag{20}$$

where sgn(.) denotes the sign function, i.e., $\mathrm{sgn}(x) = 1$ if $x>0$, $\mathrm{sgn}(x) = -1$ if $x<0$ and $\mathrm{sgn}(x) = 0$ if $x = 0$.

It can be shown that δk_a tends toward zero asymptotically by choosing a Lyapunov function to be

$$V = \frac{1}{2}\left(\frac{\mathrm{d}}{\mathrm{d}t}\delta k_a\right)^2 + \gamma\alpha\delta k_a\,\mathrm{sgn}(\delta k_a).$$

(Note that the second term of V can be thought as the potential energy of a nonlinear spring of which the stiffness is inversely proportional to the magnitude of δk_a.) Differentiation of V leads to

$$\dot{V} = -\alpha\left(\frac{\mathrm{d}}{\mathrm{d}t}\delta k_a\right)^2.$$

Since V is positive definite (therefore lower bounded) and $\dot{V}\leqslant 0$, it follows that $\dot{V}$ must tend to zero, or $(\mathrm{d}/\mathrm{d}t)\delta k_a \to 0$. Furthermore, as $(\mathrm{d}/\mathrm{d}t)\delta k_a \to 0$, it follows that $(\mathrm{d}^2/\mathrm{d}t^2)\delta k_a \to 0$, and from Eq. (20) we have $\delta k_a \to 0$.

2.3. Simulation

Eq. (20) describes the approximate dynamics of k_a under the adaptation algorithm. Numerical simulations are conducted to compare the response of the original system with the analytic solution.

Fig. 3 shows the simulation results for the system of Eqs. (1)–(8), with $m = 0.6\,\text{kg}$, $k = 296\,\text{N/m}$, $m_a = 0.08$, $b = 2$, $\alpha = 2.5$, $\alpha_1 = 4$, and $\gamma = 0.3$. The parameters of the primary structure are chosen according to the experimental apparatus shown later. The disturbance frequency is assumed to be $\omega_0 = 24.82\,\text{rad/s}$, so that the target value for k_a is 49.3. The initial value for k_a is set to be 45, and the adaptation algorithm is activated after 15 s. Fig. 3a compares the response of k_a with the solution of Eq. (20) for the same initial conditions. It is seen that the two curves match well before they are near the target value.

In deriving Eq. (20) it is assumed that ϕ switches between π and $-\pi$ instantaneously around the target value. However, in transitions the phase actually varies in a continuous way, causing small oscillations of k_a about the target value as shown in Fig. 3.

2.4. Adaptation rate

The adaptation rate of k_a is estimated as follows. Without loss of generality, assume $\delta k_a(0) < 0$. Eq. (20) becomes

$$\frac{\mathrm{d}^2}{\mathrm{d}t^2}\delta k_a + \alpha\frac{\mathrm{d}}{\mathrm{d}t}\delta k_a = \gamma\alpha. \tag{21}$$

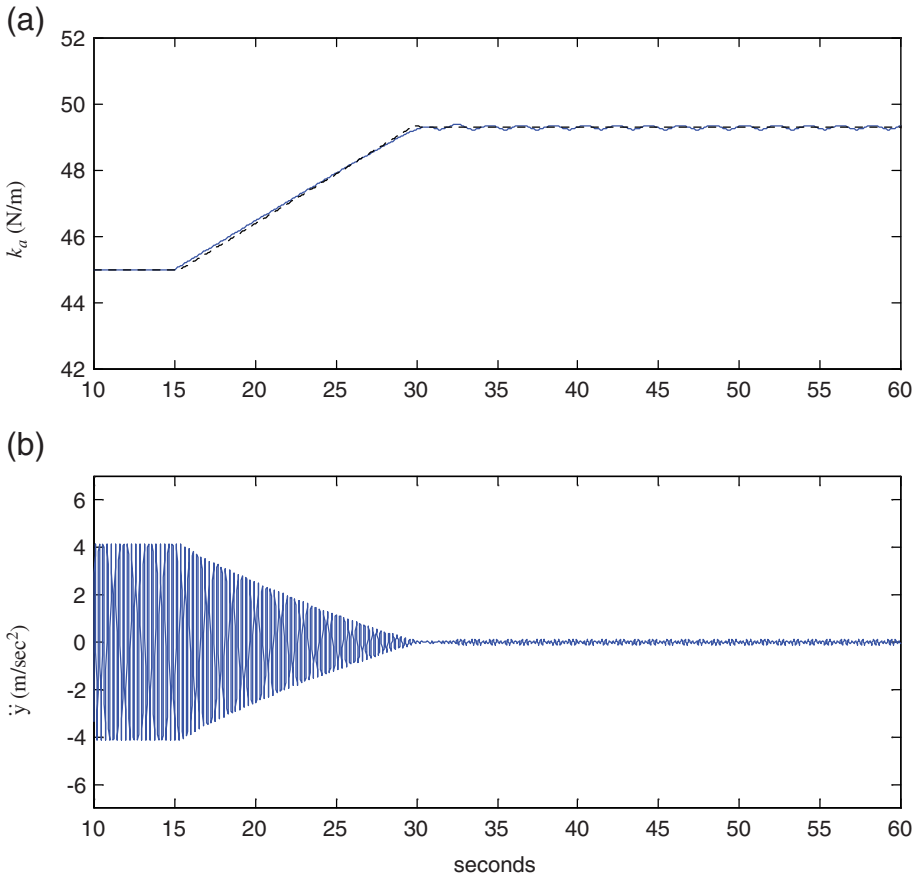

Fig. 3. Simulation results of the adaptive vibration absorber: (a) response of k_a (solid line) compared with the analytic results (dotted line); (b) accelerations ($\ddot{y}$) of the primary body.

From the above equation, $(\mathrm{d}/\mathrm{d}t)\delta k_a$ tends to be the value of γ. (It slows down abruptly as δk_a changes sign.) Hence the maximum rate of change for k_a in radian per second can be approximated to be

$$\frac{\dot{k}_a}{k_a} = \frac{\gamma}{k_a^*}. \tag{22}$$

Eq. (22) provides a criterion in the determination of γ. Since the adaptation rate should be slower than the transient response of the system, the magnitude of γ/k_a^* must be lower than the system's bandwidth.

3. Damped vibration absorber

The previous simulations show a small oscillation in k_a because the phase changes abruptly as k_a crosses k_a^*. By adding a sky-hooked dashpot to the vibration absorber, a gradual phase transition can be achieved. The damped vibration absorber is depicted in Fig. 4, for which the modified control algorithm can be expressed to be

$$u = k_a(z_1 - y) - b\dot{y}, \tag{23}$$

$$\ddot{z}_1 = \frac{k_a}{m_a}(y - z_1) - b_a\dot{z}_1, \tag{24}$$

$$\dot{k}_a = \gamma\psi_1, \tag{25}$$

$$\dot{\psi}_1 = -\alpha\psi_1 + \alpha\phi_d, \tag{26}$$

$$\phi_d = \frac{\ddot{y}}{\ddot{y}_{\mathrm{rms}}}\frac{z_1}{z_{1\,\mathrm{rms}}}, \tag{27}$$

where z_1 is the displacement of the damped vibration absorber.

To analyze the new phase detector (Eq. (27)), the transfer function between z_1 and $\ddot{y}$ is obtained from Eq. (24):

$$\frac{z_1}{\ddot{y}} = \frac{k_a}{s^2(m_a s^2 + b_a s + k_a)}. \tag{28}$$

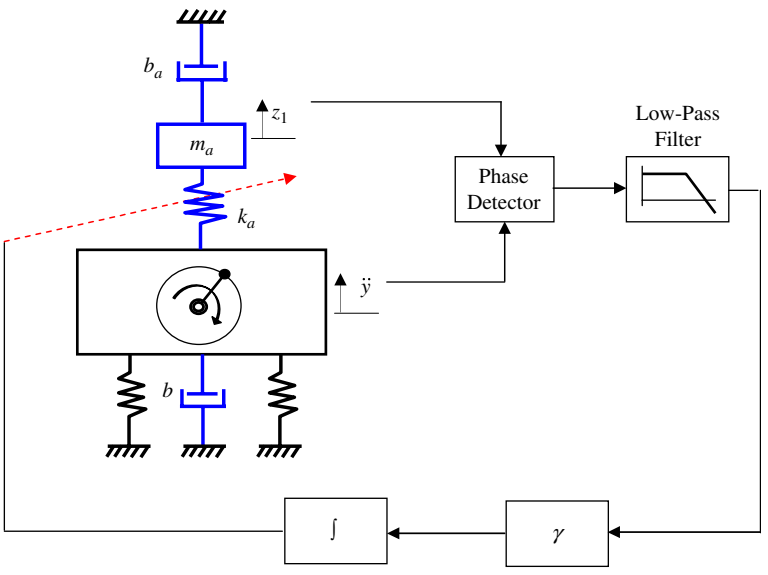

Fig. 4. Adaptive vibration absorber with a sky-hooked damper.

At the frequency ω_0, we have

$$z_1 = \frac{-k_a}{\omega_0^2(k_a - m_a\omega_0^2 + i\omega_0 b_a)}\ddot{y}. \tag{29}$$

If $\ddot{y} = a_y \sin\omega_0 t$, then from Eq. (29)

$$z_1 = -a_{z_1}\sin(\omega_0 t - \theta_1),$$

where

$$a_{z_1} = \frac{k_a}{\omega_0^2\sqrt{(k_a - m_a\omega_0^2)^2 + \omega_0^2 b_a^2}}a_y$$

and

$$\theta_1 = \tan^{-1}\left(\frac{\omega_0 b_a}{k_a - m_a\omega_0^2}\right). \tag{30}$$

(To be precise, the inverse tangent is a "four quadrant" inverse tangent, of which the range is $(-\pi, \pi)$ rather than $(-\pi/2, \pi/2)$.)

Similar to Eq. (15) the product of normalized z_1 and normalized $\ddot{y}$ can be computed to be

$$\frac{z_1}{z_{1\,\mathrm{rms}}}\frac{\ddot{y}}{\ddot{y}_{\mathrm{rms}}} = \sin(2\omega_0 t)\cos\phi_1 - \cos(2\omega_0 t)\sin\phi_1 + \sin\phi_1. \tag{31}$$

Similar to Eq. (13),

$$\phi_1 = \theta_1 - \pi/2, \tag{32}$$

which is obtained by filtering out the normalized product. In other words, if $\alpha \ll \omega_0$, Eqs. (26) and (27) can be approximated by

$$\dot{\psi}_1 = -\alpha\psi_1 + \alpha\sin\phi_1. \tag{33}$$

Since θ_1 varies continuously with k_a, so does ϕ_1.

3.1. Dynamics of k_a in the neighborhood of k_a^*

The dynamic equation for a small perturbation of k_a from the target value will be derived below.

From Eq. (30) and using the identity,

$$\frac{\mathrm{d}}{\mathrm{d}x}\tan^{-1}x = \frac{1}{1+x^2},$$

the relation between a small perturbation of θ_1 and a small perturbation of k_a can be approximated by

$$\begin{aligned}\delta\theta_1 &= \frac{\mathrm{d}}{\mathrm{d}k_a}\left(\tan^{-1}\frac{\omega_0 b_a}{k_a - m_a\omega_0^2}\right)\delta k_a = \frac{1}{1 + \left(\dfrac{\omega_0 b_a}{k_a - m_a\omega_0^2}\right)^2}\frac{-\omega_0 b_a}{(k_a - m_a\omega_0^2)^2}\delta k_a \\ &= \frac{-\omega_0 b_a}{(k_a - m_a\omega_0^2)^2 + \omega_0^2 b_a^2}\delta k_a.\end{aligned} \tag{34}$$

Since $\phi_1 = \theta_1 - \pi/2$, so that $\delta\theta_1 = \delta\phi_1$. When k_a is in the neighborhood of the target value, i.e., as $k_a/m_a \to \omega_0^2$, we have from Eq. (34)

$$\delta\phi_1 = \frac{-1}{\omega_0 b_a}\delta k_a. \tag{35}$$

From Eq. (25),

$$\frac{\mathrm{d}}{\mathrm{d}t}\delta k_a = \gamma\delta\psi_1. \tag{36}$$

As $k_a/m_a \to \omega_0^2$, $\phi_1 \to 0$, so that $\delta(\sin\phi_1) \approx \delta\phi_1$. From Eq. (33) we have

$$\frac{\mathrm{d}}{\mathrm{d}t}\delta\psi_1 = -\alpha\delta\psi_1 + \alpha\delta\phi_1. \tag{37}$$

The dynamic equation for δk_a is obtained by substituting Eqs. (35) and (36) into Eq. (37):

$$\frac{\mathrm{d}^2}{\mathrm{d}t^2}\left(\frac{1}{\gamma}\delta k_a\right) = -\frac{\alpha}{\gamma}\frac{\mathrm{d}}{\mathrm{d}t}\delta k_a - \frac{\alpha}{\omega_0 b_a}\delta k_a. \tag{38}$$

By rearranging terms, the above equation can be expressed to be

$$\frac{\mathrm{d}^2}{\mathrm{d}t^2}\delta k_a + \alpha\frac{\mathrm{d}}{\mathrm{d}t}\delta k_a + \frac{\alpha\gamma}{\omega_0 b_a}\delta k_a = 0. \tag{39}$$

3.2. Simulation

Numerical simulations are conducted to compare the response of k_a of the adaptive damped vibration absorber of Eqs. (1), (23)–(27) and that of Eq. (39). In the simulations b_a is set to be 0.013; the other parameters are the same as in the previous section. Fig. 5 shows the response of k_a and $\ddot{y}$ with a 1% deviation of initial k_a. It is seen that the trajectory of k_a matches well with solutions of the linearized model. There is no residual oscillation of k_a thanks to the additional damper.

Note that Eq. (39) is valid only when k_a is in the neighborhood of k_a^*. For large deviations Eq. (20) is still a good approximation for the damped vibration absorber. Fig. 6 shows the simulation results for an 8.5% initial error of k_a compared with the solutions of Eq. (20). The two curves match very well until k_a nears the target value. Also note the tradeoff for smoother adaptation in k_a: a higher level of residual $\ddot{y}$ due to the damper in the vibration absorber.

The above simulations show that, considering the dynamics of the overall system, k_a converges to the target value as predicted by the quasi-static model. This is because the characteristic frequency of the adaptation dynamics is set to be much lower than that of the nominal system (i.e., the non-adapted system with a constant k_a). The calculations are detailed here. The dominant poles of the nominal system in our simulations are about $-0.86 \pm 19i$. (The other poles are $-0.87 \pm 28i$.) The (lower) characteristic frequency of

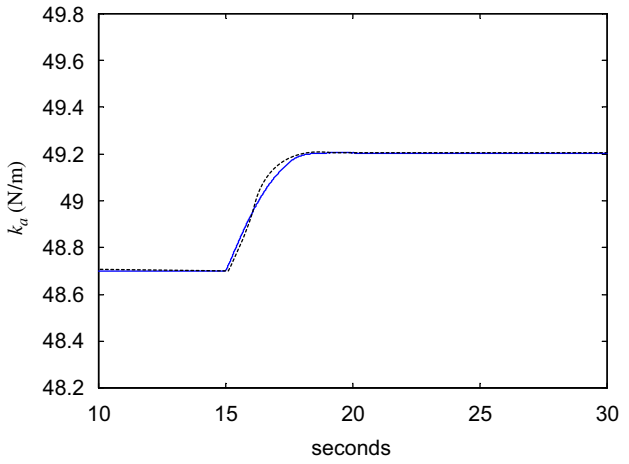

Fig. 5. Response of k_a around k_a^* for the damped adaptive vibration absorber compared with the linearized approximation (dotted line).

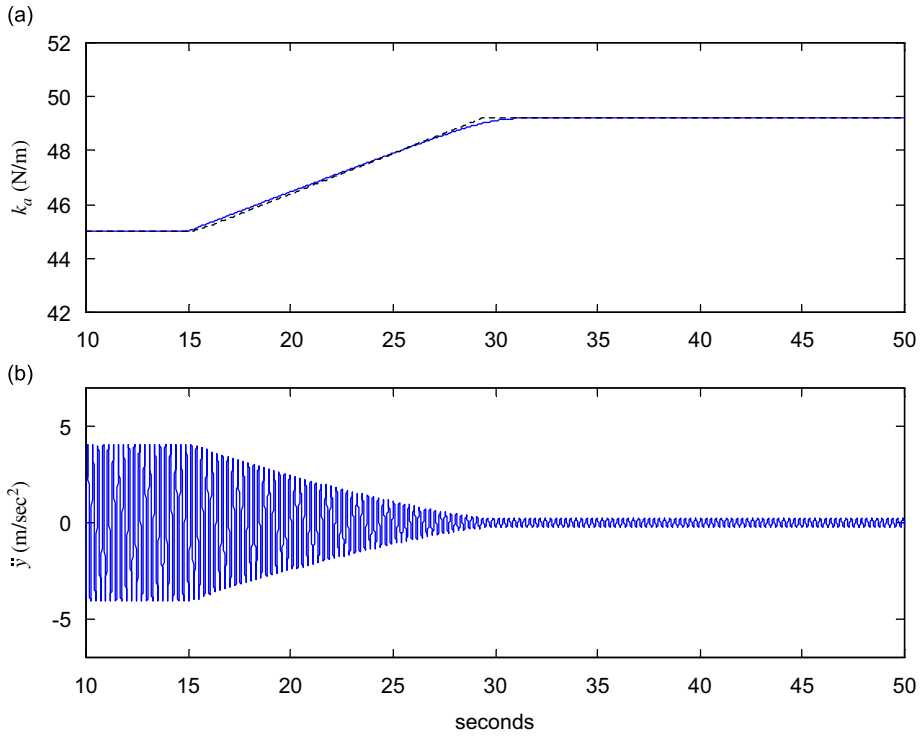

Fig. 6. Simulation results of damped adaptive vibration absorber: (a) response of k_a (with 8.5% initial deviation) compared with the solution of Eq. (20) (dotted line); (b) accelerations ($\ddot{y}$) of the primary body.

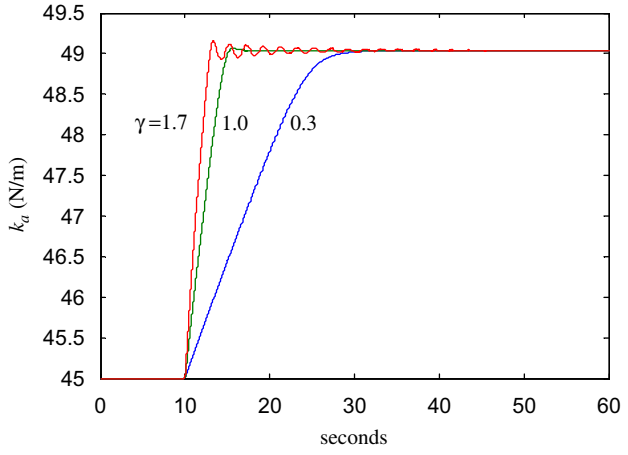

Fig. 7. Responses of k_a for γ varying from 0.3 to 1.7 (ω_n from 1 to 2.38 rad/s).

the nominal system is therefore 19 rad/s, and the real part of the dominant poles is a measure of the transient speed. From Eq. (39) the characteristic frequency of the quasi-static dynamics, denoted by ω_n, is equal to $\sqrt{\alpha\gamma/(\omega_0 b_a)}$. For the parameters used in the simulations ω_n equals 1 rad/s. If ω_n is raised too much, the slower adaptation dynamics will be coupled with the faster nominal dynamics. Fig. 7 compares the responses of k_a for γ to be 0.3, 1 and 1.7, corresponding to an ω_n of 1, 1.83 and 2.38 rad/s, respectively. It is seen that k_a starts to oscillate when ω_n is about one eighth the characteristic frequency of the nominal system.

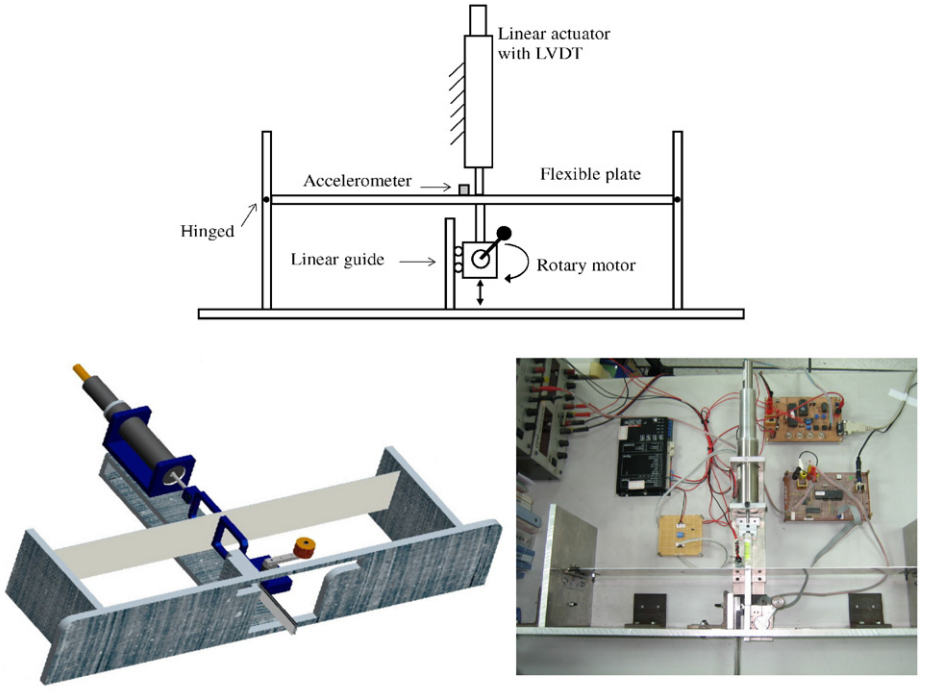

Fig. 8. Experimental setup: 2D sketch (top), 3D schematic (bottom left) and the photo (bottom right).

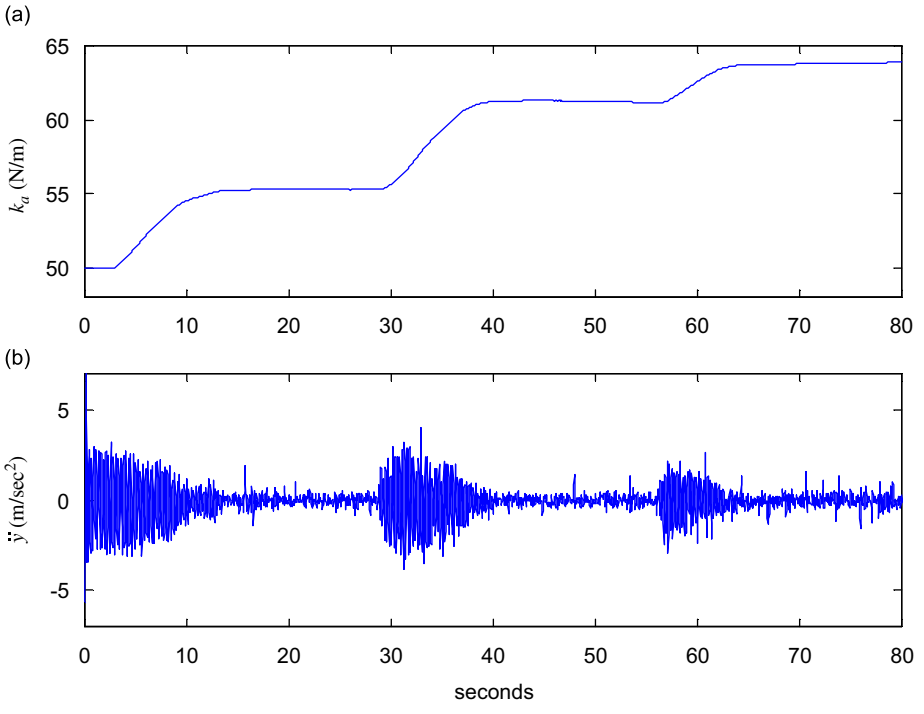

Fig. 9. Disturbance frequency arbitrarily raised at 29 and 57 s: (a) response of k_a; (b) acceleration of the primary body.

As mentioned in the previous section, γ/k_a^* should also be chosen to be much smaller than the transient rate (0.86 rad/s) of the nominal system. In the simulations γ/k_a^* is about 0.006 rad/s. Obviously it is of the lesser concern in this case.

4. Experimental results

The experimental setup is shown in Fig. 8. The inertia and the stiffness of the flexible plate are as given in Section 2. The actuator is a moving-magnet voice-coil motor equipped with an LVDT. It has a maximum stroke of 38.1 mm and a maximum continuous force of 14 N. The disturbance is generated by a rotary dc servomotor controlled by a microcontroller. A 1-G accelerometer is glued to the middle of the flexible plate. The signals of the accelerometer and the LVDT are measured through 12-bit AD converters. The control law is digitized and written in C, and is implemented on a PC running in MS-DOS mode.

Fig. 9 shows the time response with the damped adaptive absorber of Eqs. (23)–(27). In the beginning the value of k_a is fixed; the adaptation algorithm is activated after 3 s. The exciting frequency is then arbitrarily raised at 29 and 57 s. It is seen that oscillations are significantly reduced as k_a is adapted to a proper value.

5. Conclusions

By emulating the dynamics of passive mechanical elements, a virtual vibration absorber is constructed and is implemented via a linear actuator. The maximum adaptation rate for the virtual stiffness is obtained, and a linearized dynamic equation about the target value is also derived. It is shown from simulations and experiments that the analytic results are helpful in choosing the control parameters. The above development also indicates that, while the disturbance frequency is uncertain, its possible range must be known in order to devise an effective controller.

Acknowledgments

This research was supported by the National Science Council, Taiwan, ROC, under grant number NSC94-2213-E-224-032.

References

[1] M.A. Franchek, M.W. Ryan, R.J. Bernhard, Adaptive passive vibration control, *Journal of Sound and Vibration* 189 (5) (1996) 565–585.
[2] S.G. Hill, S.D. Snyder, Design of an adaptive vibration absorber to reduce electrical transformer structural vibration, *ASME Journal of Vibration and Acoustics* 124 (2002) 606–611.
[3] M.R.F. Kidner, M.J. Brennan, Varying the stiffness of a beam-like neutralizer under fuzzy logic control, *ASME Journal of Vibration and Acoustics* 124 (2002) 90–99.
[4] P. Bonello, M.J. Brennan, S.J. Elliott, Vibration control using an adaptive tuned vibration absorber with a variable curvature stiffness element, *Smart Materials and Structures* 14 (2005) 1055–1065.
[5] K. Liu, L. Liao, J. Liu, Comparison of two auto-tuning methods for a variable stiffness vibration absorber, *The Transactions of Canadian Society for Mechanical Engineering* 29 (2005) 81–96.
[6] J. Liu, K. Liu, A tunable electromagnetic vibration absorber: characterization and application, *Journal of Sound and Vibration* 295 (2006) 708–724.
[7] K.A. Williams, G.T.-C. Chiu, R.J. Bernhard, Nonlinear control of a shape memory alloy adaptive tuned vibration absorber, *Journal of Sound and Vibration* 288 (2005) 1131–1155.
[8] E. Rustighi, M.J. Brennan, B.R. Mace, Real-time control of a shape memory alloy adaptive tuned vibration absorber, *Smart Materials and Structures* 14 (2005) 1184–1195.
[9] H. Deng, X. Gong, L. Wang, Development of an adaptive tuned vibration absorber with magnetorheological elastomer, *Smart Materials and Structures* 15 (2006) N111–N116.
[10] J.S. Lai, K.W. Wang, Parametric control of structural vibrations via adaptable stiffness dynamic absorbers, *ASME Journal of Vibration and Acoustics* 118 (1996) 41–47.
[11] M. Yasuda, R. Gu, O. Nishihara, H. Matsuhisa, K. Ukai, M. Kondo, Development of anti-resonance enforced active vibration absorber system, *JSME International Journal, Series C* 39 (3) (1996) 464–469.

[12] H. Elmali, M. Renzulli, N. Olgac, Experimental comparison of delayed resonator and PD controlled vibration absorbers using electromagnetic actuators, *ASME Journal of Dynamic Systems, Measurement, and Control* 122 (2000) 514–520.
[13] G.A. Lesieutre, R. Rusovici, G.H. Koopmann, J.J. Dosch, Modelling and characterization of a piezoceramic inertial actuator, *Journal of Sound and Vibration* 261 (1) (2003) 93–107.
[14] Y. Zhang, A. Alleyne, A simple novel approach to active vibration isolation with electrohydraulic actuation, *Journal of Dynamic Systems, Measurement, and Control* 125 (2003) 125–128.
[15] Y.-D. Chen, C.-C. Fuh, P.-C. Tung, Application of voice coil motors in active dynamic vibration absorbers, *IEEE Transactions on Magnetics* 41 (3) (2005) 1149–1154.
[16] J.Q. Sun, M.R. Jolly, M.A. Norris, Passive, adaptive and active tuned vibration absorbers—a survey, *ASME Journal of Dynamic Systems, Measurement, and Control* 117 (1995) 234–242.
[17] R.P. Ma, A. Sinha, A neural-network-based active vibration absorber with state-feedback control, *Journal of Sound and Vibration* 190 (1996) 121–128.
[18] S.-T. Wu, Y.-C. Chuang, Output regulation of robot manipulators with a constantly revolving arm, *IEEE Transactions on Robotics and Automation* 19 (6) (2003) 1002–1006.
[19] S.-T. Wu, B.-Y. Chou, Speed control of a 2-dof reciprocating machine using a virtual-vibration-absorber algorithm, *JSME International Journal, Series C* 48 (2005) 674–680.
[20] S.-T. Wu, Y.-Y. Chiu, Y.-C. Yeh, Hybrid vibration absorber with virtual passive devices, *Journal of Sound and Vibration* 299 (1–2) (2007) 247–260.